Biomechanical evaluation of a Personalized External Aortic Root Support applied in the Ross procedure

Julie Vastmans[1], Heleen Fehervary[1], Peter Verbrugghe[2], Tom Verbelen[2],
Emma Vanderveken[2], Jos Vander Sloten[1], Tom Treasure[3], Filip Rega[2], and
Nele Famaey[1]

1. Biomechanics section, KU Leuven, Leuven, Belgium
2. Centre of Experimental Cardiac Surgery, KU Leuven, Leuven, Belgium
3. Clinical Operational Research Unit, UCL, London, UK

Abstract

A commonly heard concern in the Ross procedure, where a diseased aortic valve is replaced by the patient's own pulmonary valve, is the possibility of pulmonary autograft dilatation. We investigated the use of a personalized external aortic root support or exostent as a possibility for supporting the autograft from a biomechanical point of view.

In nine sheep part of the pulmonary artery was placed in aortic position. In seven of these cases, the autograft was supported by an external mesh or so-called exostent. The sheep were sacrificed six months after the procedure. Samples of the relevant tissues were obtained for subsequent mechanical testing: normal aorta, normal pulmonary artery, aorta with exostent, pulmonary artery with exostent, and pulmonary artery in aortic position for six months. After mechanical testing, the material parameters of the Gasser-Ogden-Holzapfel model were determined for the different tissue types.

Stress-strain curves of the different tissue types show significantly different mechanical behavior. At baseline stress-strain curves of the pulmonary artery are lower than aortic stress-strain curves, but at the strain levels at which the collagen fibers are recruited, the pulmonary artery behaves stiffer than the aorta. After being in aortic position for six months, the pulmonary artery tends towards aorta-like behavior. This indicates that growth and remodeling processes have taken place. When adding an exostent around the pulmonary autograft,

the mechanical behavior of the composite artery (exostent + artery) differs from the artery alone, the non-linearity being more outspoken in the former.

1. Introduction

Patients suffering from aortic valve disease can be treated by replacing their aortic valve with their own pulmonary valve, i.e. a pulmonary autograft. This procedure, known as the Ross procedure, has several advantages compared to replacement with a mechanical valve, such as better hemodynamic performance, no need for lifelong anticoagulant therapy, and the natural increase of autograft size in children [1]. Despite these advantages, possible dilatation of the autograft limits the use of this treatment [2]. Freedom from autograft reoperation in the German-Dutch Ross registry was 89.6% after ten years [3].

Schoof *et al.* demonstrated the growth and dilatation of the pulmonary autograft in growing pigs. They found that the increase in size of the pulmonary autograft is partly caused by normal growth and partly by dilatation. The authors believe that the main dilatation of the pulmonary autograft occurs at the moment the pulmonary autograft is loaded with aortic pressure. Despite the growth and dilatation, the pulmonary autograft wall still showed pulmonary characteristics both micro- and macroscopically after implantation in aortic position [4].

However, in a more recent study by the same authors on the histological evaluation of human pulmonary autograft explants, they discovered that the autograft wall showed an increase in collagen content and a reduction and fragmentation of elastin, corresponding to severe aneurysmal degeneration [5].

More recently, Rabkin-Aikawa *et al.* performed an extensive histological evaluation on human pulmonary autograft valves. These autograft valves appeared to remodel to the structure of normal aortic valves. However, the pulmonary autograft walls, associated with the valves, were structurally disrupted and not

2

well preserved [6].

Carr-White *et al.* evaluated the mechanical behavior of human pulmonary artery wall uniaxially and compared it to the normal aortic wall, noticing that the aorta is both stiffer and stronger. Additionally, they evaluated a pulmonary autograft that had been implanted for four months in a 14 year old patient, and described an increase in stiffness for this autograft, compared to pulmonary tissue [7].

When comparing the mechanical behavior of non-diseased human pulmonary and aortic roots, Azadani *et al.* performed planar biaxial experiments and found that the pulmonary artery is significantly stiffer than the aorta at systemic pressures. However, these results do not contradict the conclusions of Carr-White *et al.*, since they performed uniaxial experiments as opposed to biaxial, and they evaluate the tangent stiffness in different regions of the stress-strain curves [8].

Mookhoek *et al.* had the opportunity to mechanically evaluate dilated pulmonary autografts of 10 patients who underwent the Ross operation by equibiaxial stretch testing. They compared the mechanical behavior of the autografts with the mechanical behavior of the native aortic root, and discovered that the autografts were significantly more compliant than the native roots. The authors postulated that this decrease in vascular stiffness resulted from remodeling, and that, in this patient group, the autografts failed to remodel to represent native aortic roots at systemic pressures. However, they concluded that future research is needed to assess autograft remodeling using both normal and failed autografts [9].

In a subsequent paper by the same authors, they compared the mechanical behavior of explanted pulmonary autografts to normal pulmonary roots by equibiaxial stretch testing, noticing that pulmonary autografts are less stiff than the normal pulmonary roots [10].

To avoid dilatation of the pulmonary autograft when subjecting the pulmonary artery wall to systemic pressures, several types of reinforcements are suggested. Ungerleider *et al.* described a technique in which they place the pulmonary autograft in a Dacron graft prior to implantation in aortic position [2]. Both

Carrel *et al.* and Gebauer *et al.* proposed a similar technique, but instead of a Dacron graft, they used the sinus of the Valsalva graft [11, 12]. A case study by Kollar *et al.* reports the use of a Gore-Tex wrapping around the pulmonary autograft [13]. However, all these reinforcements are significantly stiffer than the native aorta and do not provide sufficient vascular compliance. Therefore, Nappi *et al.* proposed a resorbable reinforcement to strengthen the pulmonary autograft, which they evaluated in an ovine model [14, 15, 16, 17, 18].

Recently, a new technique was developed to reinforce the dilating aortic root in Marfan patients, i.e. a personalized external aortic root support (PEARS), as an alternative for the total root replacement or valve-sparing root replacement therapy. The PEARS is an external wrapping, which is tailored to the patient-specific geometry of the aortic root. Based on a CT or MRI of the aortic root of the patient, a replica of the patient's geometry is made by additive manu-facturing. A polyethylene terephtalate mesh with a pore size of 0.7 mm is then crimped around this replica. Next, this PEARS is surgically placed around the patient's dilated aortic root [19, 20, 21]. The initial results of this less inva-sive treatment option for Marfan patients are promising [19, 20]. The inventors claim that this method, as opposed to wrapping of aneurysms with rigid woven grafts, results in the incorporation of the soft pliant mesh in the outer layer of the aorta [20]. This claim was confirmed after an autopsy on a patient, deceased 4.5 years after he received a PEARS due to unrelated circumstances, where the incorporation of the mesh was histologically shown. Also, the aortic root of this Marfan patient showed a normal histology [21].

The mechanical performance of the PEARS mesh was studied in sheep, of which the common carotid artery was enclosed in a mesh, made of the same material as the PEARS. Four to six months after implantation, the sheep were sacri-ficed and both meshed and normal portions of the carotid artery were analyzed mechanically and histologically. Again, incorporation of the mesh in the outer arterial wall was confirmed, and the histological architecture of the arterial wall preserved. The mechanical tests were uniaxial tensile tests, starting with preconditioning, followed by stretch to failure. A significant increase in both

4

stiffness and tensile strength of the supported segments with respect to the normal carotid artery is reported [22].

In a more recent paper, Van Hoof *et al.* histologically evaluated the material of the PEARS, after it had been placed around the abdominal aorta of three sheep for a year, and compared it to the fabric used in the common vascular graft Gelweave. The PEARS material caused less disturbance to the native aortic wall compared to the material of the common vascular graft [23].

The above studies strongly suggest PEARS to be a promising method to reinforce the pulmonary autograft in the Ross procedure. To evaluate this hypothesis, this paper investigates the use of PEARS material in a simplified version of the Ross procedure in sheep. In the next sections, the surgical procedure and the mechanical characterization methodology are presented, after which the obtained results are described and discussed.

2. Materials and Methods

2.1. Surgical Procedure

A simplified version of the Ross procedure was performed on nine Lovenaar sheep: part of the thoracic aorta descendens was replaced by part of the truncus pulmonalis. In seven sheep an exostent was positioned around the pulmonary autograft. The two remaining sheep served as control sheep. After an average of 28.4 weeks the sheep were sacrificed. Before sacrifice, the maximum diameter of the aorta was measured by a CT scan. After sacrifice, the following types of tissues were harvested: normal aorta (A), reinforced aorta (AW), and reinforced pulmonary artery in aortic position (PW). In the control sheep, normal aorta (A^c), normal pulmonary artery (P^c), and pulmonary tissue in aortic position (P^c_A) were harvested. An overview of the harvested tissue types is shown in figure 1. Table 1 summarizes the details of all sheep. After removing the different tissue types, the tissues were frozen either in a physiological PBS solution or in a physiological NaCl solution, and stored at $-80°$C.

5

All experiments were approved by the Animal Ethics Committee of the KU Leuven (P053/2013).

Table 1: Details of the sheep, the bottom two sheep are the control sheep. These details include the age of the sheep at surgery, the number of weeks between the surgery and sacrifice, and the maximal diameter of autograft measured on a CT scan taken before sacrifice.

Sheep	Age implantation [weeks]	Sacrifice [weeks]	Max. diameter [mm]
BE07572-73	48.6	29.6	27.73
BE37572-385	32.4	25.9	26.01
BE37573-418	47.1	29.1	36.45
BE47572-393	33	26	29.23
BE57572-434	44.6	27.9	25.52
BE97572-0091	30.1	34.9	25.01
BE97572-0320	45	26.7	24.1
BE07572-1858	35	26.7	32.43
BE1983	31.6	28.7	52.1

2.2. Experimental protocol

First, the tissue obtained from the surgical procedure was divided into different samples. Next, sample preparation was performed including thickness measurements and marker attachment. Subsequently, the sample was mounted in a biaxial tensile testing device and mechanically loaded. The different steps are summarized in figure 2 and detailed below.

2.2.1. Sample preparation

Overnight, the tissues were thawed in a refrigerator at 4°C. After thawing, the tissue was divided into square samples of 8 mm x 8 mm for planar biaxial tests. The samples' edges were aligned with the circumferential and longitudinal direction of the vessel.

The thickness of each sample was obtained from an image in which the sample was placed between two metal plates of known thickness.

Small fragments of surgical suture wire served as markers. They were glued in the center region of the sample, where the stresses and strains are considered to be most homogeneous [26]. Four markers were placed at the corners of a square,
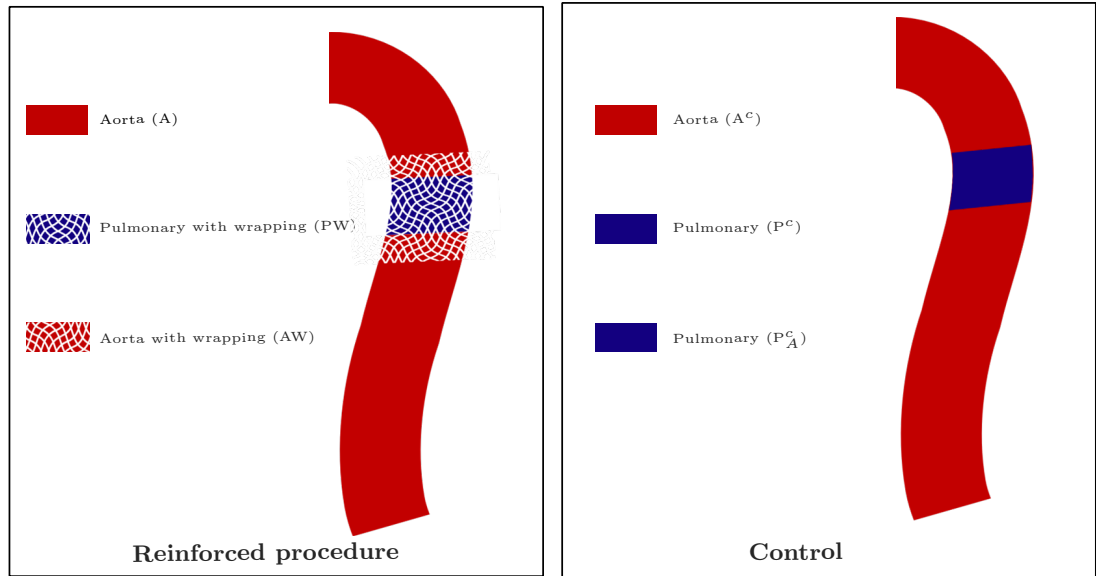
Figure 1: The left figure visualizes the full procedure where part of the thoracic descendens is replaced by a pulmonary autograft, followed by reinforcement with PEARS. The right figure visualizes the control procedure where part of the thoracic descendens is replaced by a pulmonary autograft without subsequent reinforcement
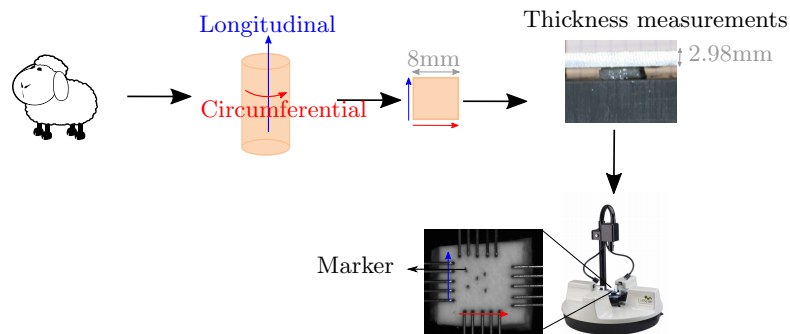

Figure 2: An overview of the different steps in the experimental protocol. A cylindrical sample is excised from the sheep, stored and then prepared into square samples. The thicknesses of these samples were then optically measured, after which biaxial testing is performed. [24, 25]

and a fifth marker was placed in the center of this square.

2.2.2. Planar biaxial tensile test

The samples were mounted in a BioTester device (CellScale, Waterloo, Canada) by means of four BioRakes. Each BioRake consists of 5 pins spaced by 1 mm, with a diameter of $300\mu m$ and a puncture length of 3 mm. The BioTester has four actuators, which can be actuated independently, and two 23N loadcells (with an accuracy of 0.2% of the full scale). A CCD camera (resolution 1280 pixels x 960 pixels) registered the sample while it is being deformed. Both the images and force measurements were taken at a sampling rate of 30Hz.
During the test, the sample was submerged into 0.9% NaCl solution at 37°C. Two types of protocols were used, which were displacement- or force-controlled. In the former, the displacement was imposed as a stretch [%] of the rakes' position. The latter imposed a force on the sample. Table 2 gives the differences between the two protocols.

Table 2: The differences between the two protocols, regarding the variable being controlled (either force or displacement), the physiological level of that variable, the prestretch being imposed (either at the beginning of each stretch or at the beginning of each set of 5 stretches), the initial distance between the rakes, and the rate at which the controlled variable was applied.

	Control	Physiological level	Prestretch	Start position	Rate rakes
P1	Force	600mN	Every, 70mN	6mm	0.3 N/s
P2	Disp	6.8%	First, 70mN	6mm	3.4 %/s

The physiological levels were determined using data from literature and Laplace's law. According to Bia *et al.*, the mean systolic blood pressure in sheep is 96 mmHg with a corresponding aortic diameter of 15.7 mm. During diastole, a blood pressure of 74.8 mmHg and a diameter of 14.7 mm is reached [27]. Laplace's law ($\sigma_{circ} = Pr/t$) allowed us to roughly estimate the circumferential stresses present in the arterial wall under physiological conditions. However, the tensile machine required force as input. Taking the width of the sample

that is loaded into account, i.e. $W = 6$ mm, the stress was converted to a force as $F = \sigma_{circ}Wt$ and with Laplace's law: $F = PrW$. This resulted in a physiological force around 600mN in the circumferential direction during systole. The physiological strain was estimated as: $\epsilon = (D_{sys} - D_{dia})/D_{dia}$ and equaled $\epsilon = 6.8\%$. The loading rate in case of the force-controlled protocol was 0.3 N/s, and the loading rate for the displacement-controlled protocol was $3.4\%/s$ [28]. These roughly estimated physiological levels, which do not account for residual stresses, were used in the testing protocols.

All protocols started with a set of 10 preconditioning cycles which were performed at half of the estimated physiological level of the displacement or the force respectively. After the preconditioning cycles, loading steps were imposed on the sample as a multitude of the physiological level calculated above. To probe the tissue's anisotropy, three different ratios of loads in the x- and y-direction were imposed per loading step on the sample: $L_x : L_y = 1 : 1, 1 : 0.5, 0.5 : 1$. In each ratio, the stretch-recover cycle was repeated five times. The final stretch step of each ratio of the last complete loading step was used for further analysis.

In the first protocol, every time a new set of five stretch cycles was started, the sample is prestretched until a load of 70 mN. In the second protocol, the prestretch was imposed before every stretch cycle with the same magnitude of 70 mN.

Figure 3 visualizes the forces that we obtain from the biaxial testing device in the circumferential and longitudinal direction. The deformation of the sample was calculated based on the position of the markers.

2.3. Constitutive modeling

The GOH model [29] is a well-known constitutive law which describes the mechanical response of arterial tissue. Two layers were considered: the media and adventitia. Since the intima's influence is negligible in the determination of solid mechanical properties, this layer was not taken into account [30]. The adventitia and the media were described as a fiber-reinforced material,
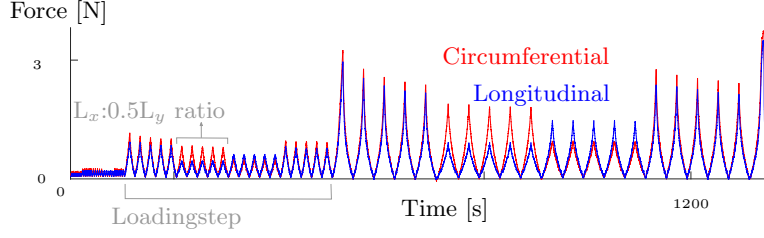
9

Figure 3: The obtained force curves in circumferential and longitudinal direction after a biaxial test, where the loadingsteps, ratios and stretch-recover cycles are apparent

consisting of a non-collagenous matrix and collagenous fibers. Ideally, both arterial layers are modeled with the same form of the strain-energy density function (SEDF) with different material parameters for each layer. However, no distinction between the different layers was made when testing the samples. Moreover, one biaxial test does not suffice for characterizing both layers simultaneously [31]. Therefore, one SEDF was used for the complete tissue. The SEDF is divided into a part modeling isotropic deformations and a part modeling anisotropic deformations:

$$\Psi(\boldsymbol{C}, \boldsymbol{a}_{01}, \boldsymbol{a}_{02}) = \Psi_{iso}(\boldsymbol{C}) + \Psi_{aniso}(\boldsymbol{C}, \boldsymbol{a}_{01}, \boldsymbol{a}_{02}). \tag{1}$$

In this equation the vectors $\boldsymbol{a}_{01}$ and $\boldsymbol{a}_{02}$ correspond to the directions of the collagen fibers, and $\boldsymbol{C} = \boldsymbol{F}^T \boldsymbol{F}$ is the right Cauchy-Green tensor where $\boldsymbol{F}$ symbolizes the deformation gradient [29, 30].

The isotropic part, associated with the mechanical response of the elastin matrix, is represented using the classic Neo-Hookean model, as $\Psi_{iso}(I_1) = C_{10}(I_1 - 3)$, with C_{10} a stress-like parameter, representing the stiffness of the matrix, and I_1 the first invariant of the right Cauchy-Green tensor.

The anisotropic part models the response of the collagen fibers as

$$\Psi_{aniso} = \frac{k_1}{2k_2} \sum_{i=4,6} \left\{ \exp\left[k_2(\kappa I_1 + (1 - 3\kappa)I_i - 1)^2 \right] - 1 \right\}, \tag{2}$$

where I_4 and I_6 correspond to the fourth and sixth invariant of the right Cauchy-Green tensor $\boldsymbol{C}$: $I_4 = \boldsymbol{C} : \boldsymbol{a}_{01} \otimes \boldsymbol{a}_{01}$ and $I_6 = \boldsymbol{C} : \boldsymbol{a}_{02} \otimes \boldsymbol{a}_{02}$. By assuming that the two fiber families are symmetrically oriented and that $F_{12} = F_{21}$, the fourth

10

and sixth invariant become equal, since

$$\boldsymbol{a}_{01} = \begin{bmatrix} \sin\alpha \\ \cos\alpha \\ 0 \end{bmatrix}, \boldsymbol{a}_{02} = \begin{bmatrix} -\sin\alpha \\ \cos\alpha \\ 0 \end{bmatrix}, \tag{3}$$

where α expresses the angle between the collagen fibers and the longitudinal direction, i.e. when $\alpha = 0$, the fibers are aligned along the longitudinal direction. k_1 relates to the stiffness of the fibers, while k_2 is linked to the nonlinear behavior of the tissue. Parameter κ includes the effect of dispersion of the collagen fibers and expresses the degree of anisotropy in the arterial layer [29, 30].

2.4. Parameter fitting

To determine the material parameters, an objective function expressing the difference between the experimentally measured forces $\boldsymbol{RF}^{exp}$, and the forces calculated based on the GOH model $\boldsymbol{RF}^{mod}$ in both directions, is minimized as

$$(\boldsymbol{R}_{11}^{mod} - \boldsymbol{R}_{11}^{exp})^2 + (\boldsymbol{R}_{22}^{mod} - \boldsymbol{R}_{22}^{exp})^2. \tag{4}$$

The experimentally measured forces $\boldsymbol{RF}^{exp}$ followed directly from the experiment. The modeled forces $\boldsymbol{RF}^{mod}$ were calculated based on the deformation gradient measured in the experiment and the SEDF explained above.

Taking the coordinates of the four outer markers, an average circumferential λ_{11} and longitudinal λ_{22} stretch were calculated. Using the incompressibility assumption, i.e. $\det(\boldsymbol{F}) = 1$, and assuming no shear due to the alignment of the material axes with the test axes, the deformation gradient $\boldsymbol{F}$ becomes

$$\boldsymbol{F} = \begin{bmatrix} \lambda_{11} & 0 & 0 \\ 0 & \lambda_{22} & 0 \\ 0 & 0 & \frac{1}{\lambda_{11}\lambda_{22}} \end{bmatrix} \tag{5}$$

Subsequently, the second Piola-Kirchhoff stress $\boldsymbol{S}_{mod}$ was calculated as

$$\boldsymbol{S}_{mod} = -\mathrm{p}\boldsymbol{C}^{-1} + 2\frac{\partial \Psi(\boldsymbol{C}^{-1})}{\partial \boldsymbol{C}}[30]. \tag{6}$$

Next, the second Piola-Kirchhoff stress $\textbf{\textit{S}}_{mod}$ was multiplied with the deformation gradient $\textbf{\textit{F}}$, resulting in the first Piola-Kirchhoff stress $\textbf{\textit{P}}_{mod}$. Finally, the modeled reaction force were determined by multiplying the first Piola-Kirchhoff stress with the undeformed area A, i.e. the initial distance between the rakes and the thickness of the sample.

The above calculations and the optimization procedure were done in *Matlab 2015a*, and the optimization procedure used to minimize the objective function was performed with *CasADi*, a freely available tool for nonlinear optimization [32]. The function *multistart* in *Matlab 2015a* was used, which allowed us to execute the optimization procedure starting from 10 different parameter sets. The ranges for the different parameters are given in table 3.

Table 3: The range of the GOH parameters. α is allowed to vary between 0 and $\pi/2$ radians, corresponding to the fibers being fully aligned to the longitudinal direction and to the circumferential direction. κ varies between 0 and 1/3 where the latter relates to a fully isotropic fiber distribution.

	C_{10} [MPa]	k_1 [MPa]	k_2 [−]	α [rad]	κ [−]
min	0	0	0	0	0
max	10	10	100	$\frac{\pi}{2}$	$\frac{1}{3}$

The material parameters are reported as a set of parameters for each specific sample, with the corresponding coefficient of determination R^2. No mean parameter set was calculated for the tissue types, since averaging is a linear operation, whereas the constitutive model is nonlinear. Robertson *et al.* showed that for nonlinear constitutive models, average coefficients often do not represent average behavior [33].

3. Results

The different parameter sets for each of the samples are given in Appendix in tables 4 to 12.

Figure 4 visualizes the boxplots for the thicknesses and the material parameters C_{10}, k_1, and k_2. No boxplots were made for the structural parameters α and κ

since they often reach their limiting values. Due to the limited number of sheep, no statistical tests were performed.

The first Piola-Kirchhoff stress was plotted for all samples in figures 5 and 6 with respect to the stretch, both in circumferential and longitudinal direction. Figure 5 pertains to the samples of the two control sheep, whereas figure 6 shows the curves of the samples of the seven sheep with exostent.
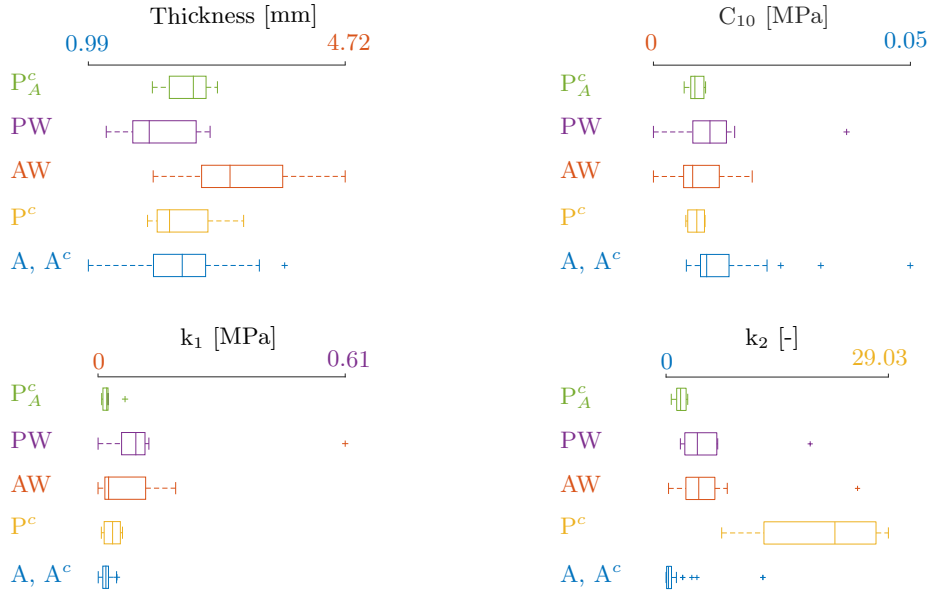

Figure 4: Boxplots of the thicknesses, and the material parameters of the GOH model for all tissue types of all sheep.

4. Discussion

In total, five different tissue types can be distinguished: normal aorta (A and A^c), normal pulmonary (P^c), aorta with exostent (AW), pulmonary with exostent (PW), and pulmonary in aorta position (P_A^c). The discussion is divided into three parts, followed by a paragraph reviewing the study limitations and future work. In the first part, we compare the normal or baseline behaviors of the pulmonary artery and aorta. The second part discusses the effect of the

Figure 5: The first Piola-Kirchhoff stress in circumferential (11) and longitudinal (22) direction for the different tissue types of the control sheep. The mechanical behavior of normal pulmonary appears to change to aorta like behavior when placed in aortic position for 6 months.
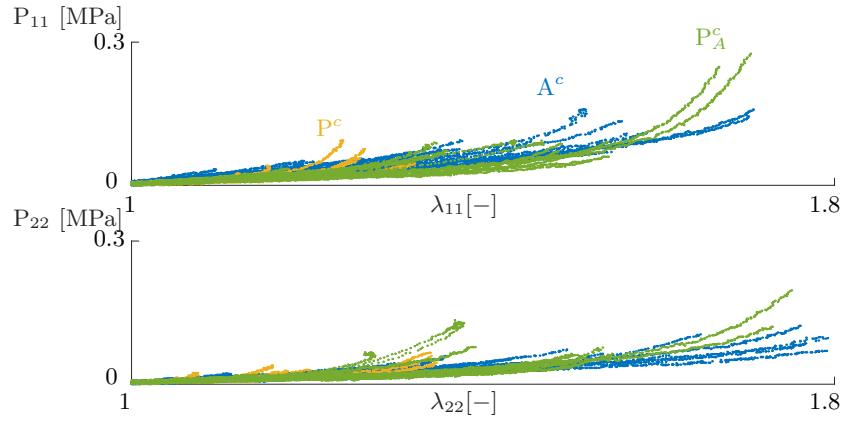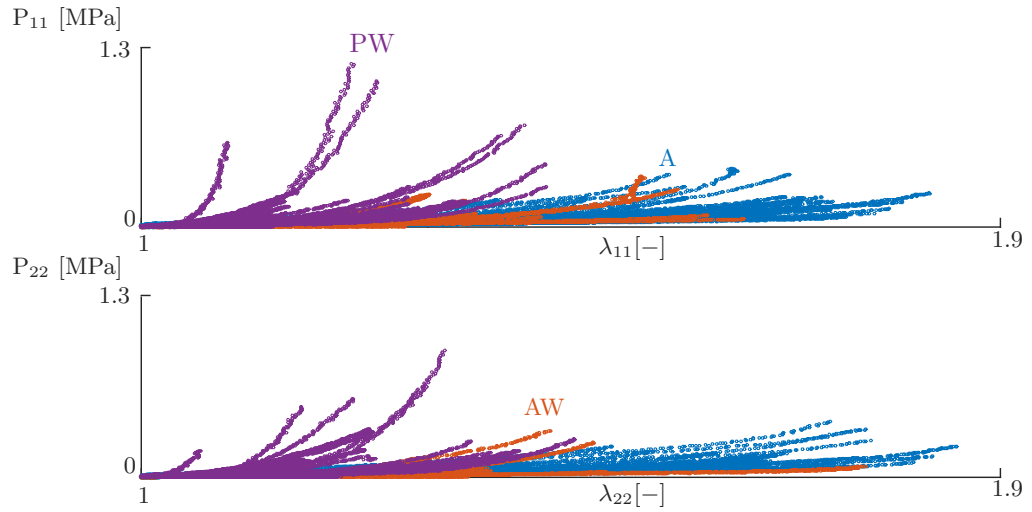

Figure 6: The first Piola-Kirchhoff stress in circumferential (11) and longitudinal (22) direction for the different tissue types of the PEARS sheep. Samples with the PEARS show a more outspoken stiffening effect, compared to their normal counterpart.

Ross procedure on the mechanical behavior of the pulmonary artery. Thirdly, the influence of the exostent is discussed.

4.1. Baseline behavior

Looking at figures 5 and 6, one can clearly distinguish the different stress-strain curves pertaining to a specific tissue type.

When comparing normal aortic behavior and pulmonary artery behavior, one can see in figure 5, that the normal pulmonary artery stiffens sooner than the normal aorta. This stiffening effect is quantified by the k_2 parameter in the material model. As can be seen in the corresponding boxplot (figure 4), this parameter appears to be higher in the pulmonary artery samples than in the normal aortic samples. Additionally, a lower initial slope of the stress-strain curves of the pulmonary arteries can be noticed when comparing it with aortic stress-strain curves. Thus, stress-strain curves of pulmonary artery samples are initially lower than the ones of the aortic samples, but when stiffening occurs, pulmonary artery samples become stiffer than aortic samples.

Contrary to our results, Carr-White *et al.* [7] divided the stress-strain curves of pulmonary artery and aortic samples in a low and high stiffness region, and found that for both regions the aorta behaved stiffer than the pulmonary artery. However, the authors performed uniaxial tests in the circumferential direction on human tissue from patients undergoing autograft surgery, with ages ranging from 10 to 59 years, as opposed to our biaxially tested samples of healthy, young sheep. On the other hand, Azadani *et al.* [8] performed similar experiments as the ones performed in this paper, and evaluated the stiffness in the systemic region for human pulmonary artery tissue and human aortic tissue of patients with a mean age of 50 years, and discovered that the pulmonary artery tissue behaves stiffer under systemic pressure. A similar conclusion can not be drawn for the young, ovine samples of this paper, since in the toe region, the stress-strain curves of aortic samples have a higher slope, whereas in the stiffening part, neither the aorta or pulmonary artery appear to behave stiffer than the other.

15

4.2. Effect of the Ross procedure

The difference in mechanical behavior between the aorta and the pulmonary artery becomes relevant when performing the Ross procedure, since loading the pulmonary artery with systemic pressure leads to different stresses in the pulmonary wall compared to loading it with pulmonary pressures, or compared to normal aorta. Consequently, a disruption in the homeostatic state of the pulmonary artery occurs, triggering growth and remodeling reactions.

It appears in figure 5 that when the pulmonary artery has been in aorta position for six months, its mechanical behavior leans more to aortic behavior. This can be an indication of remodeling, since the trend of the pulmonary artery starting to show aortic behavior when placed in aortic position, is visible.

This is contradictory to what Schoof *et al.* found, who discovered no micro- or macroscopical evidence for remodeling [4]. Moreover, Mookhoek *et al.* mechanically evaluated dilated pulmonary autografts of ten patients and compared them to the native aortic root. They found that the autografts were significantly more compliant than the native root [9]. In a follow-up paper, they compared the autografts with normal pulmonary arteries and the autografts appeared to be less stiff [10].

Contrarily, our results suggest that the pulmonary autograft starts to behave more aorta-like when positioned in aortic position. However, this discrepancy might result from the fact that Mookhoek *et al.* tested dilated pulmonary autografts, which failed to remodel [9, 10], whereas our samples appear to have remodeled.

4.3. Effect of exostent

Adding an external exostent changes the mechanical behavior of the composite (artery + exostent). Possibly, it can therefore bring the stresses in the arterial wall closer to their homeostatic value, diminishing the occurrence of growth and remodeling reactions.

As shown in figure 6, the samples with exostent material tend to stiffen sooner and more severely compared to the unreinforced samples. A slight increase in

the k_2 parameter of the wrapped aortic samples compared to the normal aortic samples supports this observation. Comparing the pulmonary samples to the wrapped pulmonary samples, one can see that the initial slope of the curve is steeper in the exostent samples than in the normal pulmonary samples. An increase in stiffness was also found by Verbrugghe *et al.*, who evaluated the microstructure, the tensile strength and the stiffness of the exostent placed around the carotid artery of sheep for four to six months.

4.4. Study Limitations

In tables 4 to 12, it is noticeable that several parameters tend to go to their limit in the parameter fitting procedure. Most often the structural parameters α, expressing the orientation of the fibers, and κ, expressing the dispersion of the fibers, reach their limit values. This can be attributed to the homogenization of the different layers in the fitting process.

The alignment of the fibers differs in the separate arterial layers. The collagen fibers in the media are closely aligned to the circumferential direction, which corresponds to an α equal to $\pi/2$, whereas in the intima and adventitia the collagen fibers are more dispersed. This different alignment may lead to difficulties in fitting this parameter. A similar conclusion was drawn by Haskett *et al.* who found that the measured fiber angle did not correspond to the fitted fiber angle of the GOH model [34]. Performing a fitting which corrects for the inhomogeneity caused by the rakes, as proposed by Fehervary *et al.* [35], and in which the different layers are considered, e.g. Badel *et al.* [36] or Vastmans *et al.* [31] might circumvent the above problem.

This study is limited to evaluating the material properties of the different tissues at two time points. In order to capture the growth and remodeling processes, more time points should be included. This can be done by taking 4D images, e.g. CT or MRI, at several time points, which can also be used to estimate material properties [37].

Finally, linking mechanical experiments on these tissues to corresponding histo-

17

logical findings, should result in considerable insight regarding the growth and remodeling processes, as well as in the incorporation of the PEARS material in the arterial wall.

4.5. Future work

In future experiments, more control sheep should be evaluated to be able to draw significant conclusions regarding growth and remodeling. Additionally, histological evaluation should be simultaneously performed to microscopically evaluate what mechanisms occur during growth and remodeling and after placing the exostent. In order to model the growth and remodeling reaction, data at different time points are needed. This data can include 4D CT or MRI images at different intervals, which allows to estimate the material properties *in vivo* and to determine the change in geometry. Finally, the prestretch which is imposed on the pulmonary autograft and on the exostent should also be measured.

5. Conclusion

The Ross procedure is a surgery in which the aortic valve is replaced by the patient's own pulmonary valve. However, due to possible dilatation of the pulmonary autograft, the use of this procedure is limited. In this study, we tested a new exostent for the pulmonary autograft in an ovine model. Several tissue types were obtained and mechanically tested.
Normal pulmonary artery has a lower slope in the low strain regions of its stress-strain curves compared to normal aorta. However, rapid stiffening takes place at lower strain levels in pulmonary artery. When placing the pulmonary artery in aortic position, its mechanical behavior changes towards more aorta-like behavior, though this result could not be proven statistically. Finally, adding the exostent around the autograft changes the behavior of the composite material severely as opposed to the baseline behavior. The stiffening effect becomes even more outspoken in the tissue samples with the exostent.

6. Acknowledgments

References

[1] J. J. M. Takkenberg, L. M. A. Klieverik, P. H. Schoof, R.-j. V. Suylen, L. A. V. Herwerden, P. E. Zondervan, M. H. Yacoub, A. J. J. C. Bogers, The Ross Procedure - A Systematic Review and Meta-Analysis, Circulation 119 (2009) 222–228. `doi:10.1161/CIRCULATIONAHA.107.726349`.

[2] R. M. Ungerleider, Y. Ootaki, I. Shen, K. F. Welke, Modified Ross Procedure to Prevent Autograft Dilatation, The Annals of Thoracic Surgery 90 (3) (2010) 1035–1037. `doi:10.1016/j.athoracsur.2009.09.078`. URL `http://dx.doi.org/10.1016/j.athoracsur.2009.09.078`

[3] E. I. Charitos, T. Hanke, U. Stierle, D. R. Robinson, A. J. J. C. Bogers, W. Hemmer, M. Bechtel, M. Misfeld, A. Gorski, J. O. Boehm, J. G. Rein, C. A. Botha, R. Lange, J. Hoerer, A. Moritz, T. Wahlers, U. F. W. Franke, M. Breuer, K. Ferrari-Kuehne, R. Hetzer, M. Huebler, G. Ziemer, J. J. M. Takkenberg, H. H. Sievers, Autograft Reinforcement to Preserve Autograft Function After the Ross Procedure - A Report From the German-Dutch Ross Registry, Circulation 120 (2009) S146–S155. `doi:10.1161/CIRCULATIONAHA.108.843391`.

[4] P. H. Schoof, M. G. Hazekamp, G. K. Van Wermeskerken, E. De Heer, J. A. Bruijn, A. C. Gittenberger-de Groot, H. A. Huysmans, Disproportionate

enlargement of the pulmonary autograft in the aortic position in growing pig, Journal of Thoracic and Cardiovascular Surgery 115 (6) (1998) 1264–1272.

[5] P. H. Schoof, J. J. M. Takkenberg, R.-j. Van Suylen, P. E. Zondervan, M. G. Hazekamp, R. A. Dion, B. A. J.J.C., Degeneration of the pulmonary autograft: An explant study, Journal of Thoracic and Cardiovascular Surgery 132 (2006) 1423–1432. `doi:10.1016/j.jtcvs.2006.07.035`.

[6] E. Rabkin-Aikawa, M. Aikawa, M. Farber, J. R. Kratz, G. Garcia-Cardena, N. T. Kouchoukos, M. B. Mitchell, R. A. Jonas, F. J. Schoen, Clinical pulmonary autograft valves: Pathologic evidence of adaptive remodeling in the aortic site, Journal of Thoracic and Cardiovascular Surgery 128 (2004) 552–561. `doi:10.1016/j.jtcvs.2004.04.016`.

[7] G. S. Carr-White, A. Afoke, E. J. Birks, S. Hughes, A. O'Halloran, S. Glennen, S. Edwards, M. Eastwood, M. H. Yacoub, Aortic Root Characteristics of Human Pulmonary Autografts, Circulation 102 (19 Suppl 3) (2000) III15–22.

[8] A. N. Azadani, S. Chitsaz, P. B. Matthews, N. Jaussaud, J. Leung, A. Wisneski, L. Ge, E. E. Tseng, Biomechanical comparison of human pulmonary and aortic roots, European Journal of Cardio-Thoracic Surgery 41 (2012) 1111–1116. `doi:10.1093/ejcts/ezr163`.

[9] A. Mookhoek, K. Krishnan, S. Chitsaz, H. Kuang, L. Ge, P. H. Schoof, A. J. J. C. Bogers, J. J. M. Takkenberg, E. E. Tseng, Biomechanics of Failed Pulmonary Autografts Compared to Native Aortic Roots, The Annals of Thoracic Surgery`doi:10.1016/j.athoracsur.2016.08.061`.
URL `http://dx.doi.org/10.1016/j.athoracsur.2016.08.061`

[10] A. Mookhoek, K. Krishnan, S. Chitsaz, H. Kuang, L. Ge, P. H. Schoof, A. J. J. C. Bogers, J. J. M. Takkenberg, E. E. Tseng, Biomechanics of Failed Pulmonary Autografts Compared With Normal Pulmonary Roots,

The Annals of Thoracic Surgery 102 (6) (2016) 1996–2002. `doi:10.1016/j.athoracsur.2016.05.010`.
URL `http://dx.doi.org/10.1016/j.athoracsur.2016.05.010`

[11] T. Carrel, A. Kadner, Long-Term Clinical and Imaging Follow-Up After Reinforced Pulmonary Autograft Ross Procedure, Seminars in Thoracic and Cardiovascular Surgery: Pediatric Cardiac Surgery Annual 19 (1) (2016) 59–62. `doi:10.1053/j.pcsu.2015.11.005`.
URL `http://dx.doi.org/10.1053/j.pcsu.2015.11.005`

[12] R. Gebauer, S. Cerny, A modification of the Ross procedure to prevent pulmonary autograft dilatation 36 (2009) 195–197. `doi:10.1016/j.ejcts.2009.03.009`.

[13] A. C. Kollar, S. D. Lick, D. M. Palacio, R. F. Johnson, Ross Procedure With a Composite Autograft Using Stretch Gore-Tex Material, Annals of Thoracic Surgery 88 (2009) e34–e36. `doi:10.1016/j.athoracsur.2009.06.117`.
URL `http://dx.doi.org/10.1016/j.athoracsur.2009.06.117`

[14] F. Nappi, C. Spadaccio, C. Castaldo, F. Di Meglio, D. Nurzynska, S. Montagnani, M. Chello, C. Acar, Reinforcement of the Pulmonary Artery Autograft with a Polyglactin and Polydioxanone Mesh in the Ross Operation: Experimental Study in Growing Lamb, The Journal of Heart Valve Disease 23 (2014) 145–148.

[15] F. Nappi, C. Spadaccio, M. Fraldi, C. Acar, Use of bioresorbable scaffold for neopulmonary artery in simple transposition of great arteries : Tissue engineering moves steps in pediatric cardiac surgery, International Journal of Cardiology 201 (2015) 639–643. `doi:10.1016/j.ijcard.2015.08.124`.
URL `http://dx.doi.org/10.1016/j.ijcard.2015.08.124`

[16] F. Nappi, C. Spadaccio, P. Fouret, N. Hammoudi, C. Chachques, M. Chello, C. Acar, An experimental model of the Ross operation : Development

of resorbable reinforcements for pulmonary autografts, The Journal of Thoracic and Cardiovascular Surgery 149 (4) (2015) 1134–1142. `doi: 10.1016/j.jtcvs.2014.12.056`.
URL `http://dx.doi.org/10.1016/j.jtcvs.2014.12.056`

[17] F. Nappi, A. R. Donato, D. Di Vito, C. Spadaccio, C. Acar, M. Fraldi, Stress-shielding, growth and remodeling of pulmonary artery reinforced with copolymer scaffold and transposed into aortic position, Biomechanics and Modeling in Mechanobiology 15 (5) (2016) 1141–1157. `doi:10.1007/ s10237-015-0749-y`.

[18] F. Nappi, C. Spadaccio, M. Fraldi, S. Montagnani, P. Fouret, C. Chachques, A composite semiresorbable armoured scaffold stabilizes pulmonary autograft after the Ross operation : Mr Ross's dream fulfilled, The Journal of Thoracic and Cardiovascular Surgery 151 (1) (2016) 155–164.e1. `doi:10.1016/j.jtcvs.2015.09.084`.
URL `http://dx.doi.org/10.1016/j.jtcvs.2015.09.084`

[19] J. Pepper, K. M. J. Chan, J. Gavino, T. Golesworthy, R. Mohiaddin, T. Treasure, External aortic root support for Marfan syndrome: early clinical results in the first 20 recipients with a bespoke implant, Journal of the Royal Society of Medicine (2010) 1–6`doi:10.1258/jrsm.2010.100070`.

[20] T. Treasure, J. J. M. Takkenberg, T. Golesworthy, F. Rega, M. Petrou, U. Rosendahl, R. Mohiaddin, M. Rubens, W. Thornton, B. Lees, J. Pepper, Personalised external aortic root support (PEARS) in Marfan syndrome: analysis of 1 $$ 9 year outcomes by intention-to-treat in a cohort of the first 30 consecutive patients to receive a novel tissue and valve-conserving procedure, compared with the publ, Heart 100 (12) (2014) 969–975. `doi: 10.1136/heartjnl-2013-304913`.

[21] J. Pepper, M. Goddard, R. Mohiaddin, T. Treasure, Histology of a Marfan aorta 4,5 years after personalized external aortic root support, Eu-

ropean Journal of Cardio-Thoracic Surgery 48 (2015) 502–505. `doi: 10.1093/ejcts/ezu415`.

[22] P. Verbrugghe, E. Verbeken, J. Pepper, T. Treasure, B. Meyns, B. Meuris, P. Herijgers, F. Rega, External aortic root support: a histological and mechanical study, Interactive CardioVascular and Thoracic Surgery 17 (April) (2013) 334–339. `doi:10.1093/icvts/ivt165`.

[23] L. Van Hoof, P. Verbrugghe, E. Verbeken, T. Treasure, N. Famaey, B. Meuris, P. Herijgers, F. Rega, External aortic support: histological comparison of low porosity graft material and a macroporous mesh in sheep 12 months after implantation, Interactive CardioVascular and Thoracic Surgery.

[24] Clipart Panda.
URL `http://www.clipartpanda.com/categories/lamb-clipart-black-and-white`

[25] CellScale Biomaterials Testing, BioTester Biaxial Test System - User Manual.

[26] M. S. Sacks, Biaxial Mechanical Evaluation of Planar Biological Materials, Journal of elasticity 61 (2000) 199–246.

[27] D. Bia, R. L. Armentano, J. C. Grignola, D. Craiem, Y. A. Zócalo, F. F. Ginés, J. Levenson, The Vascular Smooth Muscle of Great Arteries: Local Control Site of Arterial Buffering Function?, Revista Espanola de Cardiologia 56 (12) (2003) 1202–1209.

[28] M. Van den Abbeele, M. Smoljkić, H. Fehervary, S. Verleden, N. Famaey, J. Vander Sloten, Characterisation of mechanical properties of human pulmonary and aortic tissue, IFMBE Proceedings 45 (2014) 387–390.

[29] T. C. Gasser, R. W. Ogden, G. A. Holzapfel, Hyperelastic modelling of arterial layers with distributed collagen fibre orientations., Journal of the

Royal Society, Interface / the Royal Society 3 (6) (2006) 15–35. `arXiv:`
`0312002v1`, `doi:10.1098/rsif.2005.0073`.

[30] G. A. Holzapfel, T. C. Gasser, R. W. Ogden, A new constitutive framework
for arterial wall mechanics and a comparative study of material models,
Journal of elasticity (2000) 1–48`arXiv:A:1010835316564`, `doi:10.1023/`
`A:1010835316564`.
URL `http://www.springerlink.com/index/Q1185464175U2738.pdf`

[31] J. Vastmans, H. Fehervary, M. Smoljkić, J. Vander Sloten, N. Famaey, De-
termination of layer-specific properties through planar biaxial and uniaxial
tensile tests on intact arterial tissue, In preparation.

[32] J. Andersson, A General-Purpose Software Framework for Dynamic Opti-
mization, PhD thesis, Arenberg Doctoral School, KU Leuven, Department
of Electrical Engineering (ESAT/SCD) and Optimization in Engineering
Center, Kasteelpark Arenberg 10, 3001-Heverlee, Belgium (October 2013).

[33] D. Robertson, D. Cook, Unrealistic statistics: How average constitutive
coefficients can produce non-physical results, Journal of the Mechanical
Behavior of Biomedical Materials 40 (2014) 234–239. `doi:10.1016/j.`
`jmbbm.2014.09.006`.

[34] D. Haskett, G. Johnson, A. Zhou, U. Utzinger, J. Vande, Microstructural
and biomechanical alterations of the human aorta as a function of age and
location, Biomechanics and Modeling in Mechanobiology 9 (6) (2010) 725–
736. `doi:10.1007/s10237-010-0209-7`.

[35] H. Fehervary, M. Smoljkic, J. Vander Sloten, N. Famaey, Planar biaxial
testing of soft biological tissue using rakes: A critical analysis of proto-
col and fitting process, Journal of the Mechanical Behavior of Biomedical
Materials 61 (2016) 135–151. `doi:10.1016/j.jmbbm.2016.01.011`.

[36] P. Badel, S. Avril, S. Lessner, M. Sutton, P. Badel, S. Avril, S. Lessner,
M. Sutton, Mechanical identification of layer-specific properties of mouse

24

carotid arteries using 3D-DIC and a hyperelastic anisotropic constitutive model, Computer Methods in Biomechanics and Biomedical Engineering 15 (1) (2012) 37–48. `doi:10.1080/10255842.2011.586945`.

[37] M. Smoljkić, J. Vander Sloten, P. Segers, N. Famaey, Non-invasive, energy-based assessment of patient-specific material properties of arterial tissue, Biomechanics and Modeling in Mechanobiology 14 (5) (2015) 1045–1056. `doi:10.1007/s10237-015-0653-5`.

Appendix

Table 4: Coefficients of constitutive modeling for sheep BE07572-73

	Sample No	Protocol	C_{10} $[MPa]$	k_1 $[MPa]$	k_2 $[-]$	α $[rad]$	κ $[-]$	thickness $[mm]$	R^2 $[-]$
	Sample 1	P1	0.0305	0.0289	1.2315	1.569	0.2764	1.3973	0.9873
	Sample 2	P1	0.0468	0.0468	1.35	1.5678	0.3153	1.0817	0.9900
Aorta	Sample 3	P2	0.0146	0.0333	0.1688	1.5686	0.305	1.6512	0.9644
	Sample 4	P1	0.0232	0.014	$5.55e^{-6}$	1.2737	$1.06e^{-7}$	1.928	0.1082
	Sample 5	P2	0.0123	0.0458	0.2378	1.5698	0.3025	1.7761	0.9697
Aorta Wrapped	Sample 1	P2	0	0	7.992	0.1006	0.3212	4.7221	-2.3964
	Sample 1	P2	0.0148	0.1255	4.0845	0.0002	0.2999	1.2467	0.8993
Pulmonary Wrapped	Sample2	P1	$1.16e^{-8}$	$1.52e^{-4}$	2.5058	0.7937	$3.56e^{-5}$	1.7572	0.6828
	Sample3	P2	0.0096	0.0734	1.8683	1.5707	0.0929	1.3793	0.9813

Table 5: Coefficients of constitutive modeling for sheep BE37572-385, * due to hardware problems, this sample was mounted three times

	Sample No	Protocol	C_{10} $[MPa]$	k_1 $[MPa]$	k_2 $[-]$	α $[rad]$	κ $[-]$	thickness $[mm]$	R^2 $[-]$
	Sample 1	P1	0.0207	0.0067	12.6338	1.5693	0.2119	1.874	0.9192
	Sample 2	P1	0.0097	0.0207	0.8264	1.5657	0.2396	2.5115	0.9493
Aorta	Sample 3	P2	0.0062	0.0227	0.0285	1.5672	0.3221	3.1707	0.9701
	Sample 4	P2	0.0089	0.0253	0.2587	1.5688	0.2987	2.2844	0.9813
	Sample 5	P1	0.0129	0.0024	12.6498	1.5679	0.1927	2.7264	0.8978
	Sample 6	P2	0.0064	0.0062	3.3626	1.5701	0.194	3.4736	0.9515
Aorta Wrapped	Sample 1	P1	0.018	0.0276	25.0024	1.5701	$7.92e^{-7}$	2.6336	0.9216
	Sample 2	P2	0.0039	0.1916	4.7558	1.5706	0.2946	3.7131	0.9503
Pulmonary Wrapped	Sample 1*	P2	0.0103	0.1127	5.4795	1.5707	0.1983	1.7171	0.9828

Table 6: Coefficients of constitutive modeling for sheep BE37572-418

	Sample No	Protocol	C_{10} $[MPa]$	k_1 $[MPa]$	k_2 $[-]$	α $[rad]$	κ $[-]$	thickness $[mm]$	R^2 $[-]$
	Sample 1	P1	0.0069	0.0052	0.1585	0.8733	$7.95e^{-6}$	3.4374	0.9808
Aorta	Sample 2	P1	0.016	0.018	2.1516	1.5686	0.3093	2.187	0.9630
	Sample 3	P2	0.0093	0.0269	0.5303	1.5681	0.2929	2.5041	0.9822
	Sample 4	P2	0.0091	0.0281	0.3094	1.5701	0.2819	2.5152	0.9753
Aorta Wrapped	Sample 1	P2	0.012	0.1696	2.2527	1.5636	0.3332	1.9294	0.9328
Pulmonary Wrapped	Sample 1	P1	$5.12e^{-4}$	0.0988	2.6545	0.5387	$4.11e^{-7}$	2.6519	0.9015

Table 7: Coefficients of constitutive modeling for sheep BE47572-393

	Sample No	Protocol	C_{10} [MPa]	k_1 [MPa]	k_2 [−]	α [rad]	κ [−]	thickness [mm]	R^2 [−]
Aorta	Sample 1	P2	0.0135	0.0303	0.469	1.5692	0.2911	1.7213	0.9647
	Sample 2	P1	0.0178	0.0276	0.6686	0.9976	0.2119	1.8815	0.9802
	Sample 3	P1	0.0196	0.0108	$6.46e^{-6}$	1.2469	$1.31e^{-7}$	2.3534	0.0391
	Sample 4	P2	0.0083	0.0248	0.0355	1.5678	0.2783	2.7873	0.9684
	Sample 5	P1	0.0069	0.0294	0.336	1.5697	0.2722	0.9864	0.9247
Aorta Wrapped	Sample 1	P1	0.0095	0.0247	2.3126	1.0473	$4.07e^{-7}$	2.1584	0.9937
	Sample 2	P2	0.007	0.1175	6.93	0.0006	0.3217	3.8133	0.9540

Table 8: Coefficients of constitutive modeling for sheep BE57572-434

	Sample No	Protocol	C_{10} [MPa]	k_1 [MPa]	k_2 [−]	α [rad]	κ [−]	thickness [mm]	R^2 [−]
Aorta	Sample 1	P1	0.0071	0.0028	$4.65e^{-5}$	1.5701	$5.76e^{-7}$	3.4149	0.8725
	Sample 2	P1	0.0105	0.0052	0.372	1.0009	$6.25e^{-9}$	2.5347	0.9789
	Sample 3	P2	0.0089	0.0215	$1.98e^{-6}$	1.565	0.3243	3.8418	0.9732
Aorta Wrapped	Sample 1	P2	0.0073	0.032	3.952	1.5703	0.2779	3.09	0.9731
Pulmonary Wrapped	Sample 1	P2	0.0094	0.0933	6.5858	1.5704	0.2514	2.4903	0.9828

Table 9: Coefficients of constitutive modeling for sheep BE97572-0091

	Sample No	Protocol	C_{10} [MPa]	k_1 [MPa]	k_2 [−]	α [rad]	κ [−]	thickness [mm]	R^2 [−]
Aorta	Sample 1	P1	0.0087	0.019	0.1066	1.0247	0.0617	1.9391	0.9621
	Sample 2	P2	0.0095	0.0233	$2.86e^{-6}$	1.57	0.2386	2.5462	0.9730
	Sample 3	P2	0.0115	0.0198	$4.06e^{-7}$	0.3167	0.2274	2.2482	0.9778
Aorta Wrapped	Sample 1	P1	0.0143	0.0152	4.5826	1.5698	$7.81e^{-7}$	2.9763	0.9498
	Sample 2	P2	0.0055	0.019	2.9208	1.5702	0.2373	3.0039	0.9466
Pulmonary Wrapped	Sample 1	P2	0.0128	0.0782	6.7432	0.0002	0.2545	1.872	0.9606
	Sample2	P1	0.0128	0.0124	2.2748	0.8047	$1.70e^{-6}$	1.7677	0.9803

Table 10: Coefficients of constitutive modeling for sheep BE97572-320

	Sample No	Protocol	C_{10} [MPa]	k_1 [MPa]	k_2 [−]	α [rad]	κ [−]	thickness [mm]	R^2 [−]
Aorta	Sample 1	P1	0.0149	0.0166	2.1845	1.568	0.2527	2.6246	0.9734
	Sample 2	P2	0.01	0.041	0.0956	1.5688	0.3133	2.281	0.9730
	Sample 3	P1	0.01	0.017	0.1512	0.917	$1.50e^{-6}$	1.5266	0.9754
Aorta Wrapped	Sample 1	P2	0.007	0.0169	0.3214	1.5676	0.2963	3.9786	0.9653
Pulmonary Wrapped	Sample 1	P1	0.0352	0.61	18.821	1.5703	0.2767	2.522	0.8947

Table 11: Coefficients of constitutive modeling for control sheep BE07572-1858

	Sample No	Protocol	C_{10} $[MPa]$	k_1 $[MPa]$	k_2 $[-]$	α $[rad]$	κ $[-]$	thickness $[mm]$	R^2 $[-]$
Aorta	Sample 1	P1	0.015	0.0139	$7.21e^{-7}$	1.3129	$6.83e^{-8}$	2.3519	0.9236
	Sample 2	P1	0.0069	0.0104	0.3886	0.9932	$6.43e^{-7}$	2.2967	0.9745
	Sample 3	P2	0.0104	0.0254	0.1306	1.5698	0.2699	1.9356	0.9646
	Sample 4	P2	0.0089	0.0225	0.0796	1.3212	0.2433	2.0688	0.9656
	Sample 5	P1	0.006	0.0151	0.2576	1.0343	$4.25e^{-7}$	2.1482	0.9430
	Sample 6	P1	0.0099	0.0081	0.4995	0.9339	$4.10e^{-6}$	2.1613	0.9808
Pulmonary	Sample 1	P2	0.0092	0.0498	29.0313	0.7647	0.3333	2.2068	0.8962
	Sample 2	P1	0.0094	0.0221	18.2967	1.57	0.2507	1.847	0.9638
Pulmonary in AP	Sample 1	P2	0.0068	0.0247	2.6176	1.57	0.2553	2.1642	0.9166

Table 12: Coefficients of constitutive modeling for sheep BE1983

	Sample No	Protocol	C_{10} $[MPa]$	k_1 $[MPa]$	k_2 $[-]$	α $[rad]$	κ $[-]$	thickness $[mm]$	R^2 $[-]$
Aorta	Sample 1	P2	0.0085	0.0151	0.4489	1.5702	0.1835	2.6469	0.9696
	Sample 2	P2	0.0096	0.0175	1.2951	1.5701	0.2304	2.6802	0.9637
	Sample 3	P1	0.0091	0.0215	0.4496	1.5692	0.2628	2.6702	0.9677
	Sample 4	P2	0.0125	0.0206	4.0298	1.5685	0.3047	2.7782	0.9616
	Sample 5	P1	0.0086	0.0121	0.4422	1.0876	0.1517	3.077	0.9751
	Sample 6	P2	0.0072	0.0194	0.0117	1.5693	0.2614	3.4658	0.9569
Pulmonary	Sample 1	P2	0.0059	0.0604	7.262	1.5703	0.3066	2.1276	0.8554
	Sample 2	P1	0.0066	0.0082	25.8	1.5678	0.2283	3.2446	0.8841
Pulmonary in AP	Sample 1	P2	0.0069	0.0099	2.827	1.5701	0.2637	2.6984	0.9546
	Sample2	P2	0.0095	0.0245	0.6802	1.5703	0.2752	1.9176	0.8857
	Sample3	P2	0.0056	0.0121	2.035	1.5695	0.2735	2.4794	0.9591
	Sample4	P1	0.0092	0.0667	1.7638	0.0003	0.2757	2.8639	0.8657
	Sample5	P2	0.0082	0.0184	1.3865	1.5687	0.3026	2.5475	0.9738